Molecular Interactions of N-RAP, a Nebulin-Related Protein of Striated Muscle Myotendon Junctions and Intercalated Disks

Gang Luo, Amy H. Herrera, and Robert Horowits*

Laboratory of Physical Biology, National Institute of Arthritis and Musculoskeletal and Skin Diseases, National Institutes of Health, Bethesda, Maryland 20892

Received October 7, 1998; Revised Manuscript Received February 1, 1999

ABSTRACT: N-RAP is a recently discovered muscle-specific protein that is concentrated at the myotendon junctions in skeletal muscle and at the intercalated disks in cardiac muscle. The C-terminal half of N-RAP contains a region with sequence homology to nebulin, while a LIM domain is found at its N-terminus. N-RAP is hypothesized to perform an anchoring function, linking the terminal actin filaments of myofibrils to protein complexes located beneath the sarcolemma. We used a solid-phase assay to screen myofibrillar and junctional proteins for binding to several recombinant fragments of N-RAP, including the nebulin-like super repeat region (N-RAP-SR), the N-terminal half including the LIM domain (N-RAP-NH), and the region of N-RAP between the super repeat region and the LIM domain (N-RAP-IB). Actin is the only myofibrillar protein tested that exhibits specific binding to N-RAP, with high-affinity binding to N-RAP super repeats, and 10-fold weaker binding to N-RAP-IB. In contrast, myosin, isolated myosin heads, tropomyosin, and troponin exhibited no specific interaction with N-RAP domains. A recombinant fragment corresponding to the C-terminal one-fourth of vinculin also binds specifically to N-RAP super repeats, while no specific N-RAP binding activity was observed for other regions of the vinculin molecule. Finally, talin binds with high affinity to the LIM domain of N-RAP. These results support our hypothesis that N-RAP is part of a complex of proteins that anchors the terminal actin filaments of the myofibril to the membrane, and functions in transmitting tension from the myofibrils to the extracellular matrix.

We recently discovered N-RAP, a novel protein found in skeletal and cardiac muscles (*1*). The C-terminal half of mouse N-RAP contains 587 residues that share 44% amino acid identity with human nebulin, a giant actin-binding protein found in skeletal muscles. Mimicking the organization of nebulin (*2*−*5*), the nebulin-related region of N-RAP consists of 17 weakly repeating ∼35 residue modules; the modules are in turn organized into more highly conserved super repeats, with each super repeat containing 7 modules (*1*). In contrast, the ∼800 000 dalton nebulin polypeptide contains more than 20 super repeats (*3, 4*), and stretches along nearly the entire length of the sarcomeric actin filaments in skeletal muscle (*6*). Naturally occurring variations in nebulin size are correlated with thin filament length, supporting the hypothesis that nebulin regulates the length of actin filaments (*2, 7*).

In addition to the N-RAP super repeat region, N-RAP contains the consensus sequence for an N-terminal LIM domain (*1*). LIM domains are cysteine-rich regions that bind two zinc ions, resulting in the formation of two adjacent zinc finger-like structures (*8, 9*). They are found in a diverse group of proteins, including transcription factors and cytoskeletal proteins. Unlike zinc finger domains that bind DNA, the primary role of LIM domains appears to be to mediate protein−protein interactions (*8, 9*).

* Address correspondence to this author at Building 6, Room 408, MSC 2755, National Institutes of Health, Bethesda, MD 20892-2755. Telephone: 301-435-8371. Fax: 301-402-0009. E-mail: horowits@helix.nih.gov.

Our initial study showed that N-RAP is concentrated at the longitudinal ends of the myofibrils (*1*). In skeletal muscles, this is the myotendon junction, while in cardiac muscle this region is the intercalated disk. In both tissues, these are sites of mechanical coupling between the myofibrils and the cell membrane (*10*−*12*). On the basis of its domain organization and subcellular localization, we hypothesized that N-RAP may serve a mechanical role, linking the terminal actin filaments of myofibrils to the specific proteins concentrated in these junctional regions (*1*).

Here we report the use of a solid-phase binding assay to screen various candidate proteins for the ability to bind to specific regions of mouse N-RAP. The results demonstrate specific interactions between defined regions of N-RAP and actin, talin, and vinculin. Talin (*13*) and vinculin (*14*) are concentrated at myotendon junctions, where they are believed to link myofibrillar actin filaments to the cell membrane. Therefore, our results suggest that N-RAP is an integral component of the complex of proteins found at myofibril termini, consistent with the hypothesis that it plays a mechanical role in the transmission of tension to the sarcolemma (schematized in Figure 11).

MATERIALS AND METHODS

Expression and Purification of N-RAP Fragments. Recombinant mouse N-RAP fragments containing an N-terminal histidine tag were expressed in *E. coli* and purified as previously described (*1*). In brief, cDNA fragments encoding defined regions of N-RAP were PCR-amplified

10.1021/bi982395t
Published on Web 04/22/1999

from a mouse skeletal muscle cDNA pool using the GIBCO BRL Elongase enzyme mix (Life Technologies, Inc., Gaithersburg, MD). The amplified N-RAP cDNAs were subsequently cloned into the GIBCO BRL pProEX-1 expression vector. BL21(DE3) pLysS *E. coli* cells were used as hosts for protein expression (Novagen, Inc., Madison, WI). The expressed histidine-tagged N-RAP fragments were purified with Ni−NTA resin (Qiagen, Inc., Chatsworth, CA) in the presence of 6 M urea. A plasmid consisting of the pProEX HTa vector with an insert encoding chloramphenicol acetyltransferase was purchased from GIBCO BRL and used to express and purify histidine-tagged chloramphenicol acetyltransferase (HIS-CAT) as described above.

Proteins Assayed for N-RAP Binding Activity. Glutathione *S*-transferase (GST)-tagged recombinant chicken vinculin fragments were provided by Dr. Susan W. Craig of Johns Hopkins University. The recombinant vinculin fragments were GST/V1−430, GST/V431−850, and GST/V811−1066, where the numerical suffixes indicate the residues of the chicken vinculin sequence that are included in the constructs. These recombinant vinculin fusion constructs have been described by Johnson and Craig (*15*) and by Adey and Kay (*16*), but are all original products of the Craig laboratory.

Talin purified from human platelets was provided by Dr. Keith Burridge (University of North Carolina) (*17*). Actin purified from rabbit skeletal muscle (*18*) was provided by Dr. James Sellers (NHLBI, National Institutes of Health). Purified troponin-T and reconstituted troponin complex from rabbit skeletal muscle (*19*), as well as tropomyosin (*18*), were provided by Dr. Mingda She (NIAMS, National Institutes of Health). Myosin and isolated myosin heads (S1) from rabbit skeletal muscle were provided by Dr. Ling Xie (NIAMS, National Institutes of Health) (*20*).

Antibodies. Monoclonal anti-actin antibody was purchased from Boehringer Mannheim Corp. (Indianapolis, IN). Monoclonal anti-troponin-T and anti-talin as well as polyclonal anti-myosin and anti-tropomyosin antibodies were purchased from Sigma Chemical Co. (St. Louis, MO). Polyclonal anti-GST antibody was purchased from Calbiochem (San Diego, CA). Horseradish peroxidase-linked donkey anti-rabbit and anti-mouse whole antibodies were purchased from Amersham Corp. (Arlington Heights, IL), and were used as secondary antibodies to detect the polyclonal and monoclonal antibodies, respectively. Antibodies against actin, talin, and GST were used at a dilution of 1:2000; antbodies against troponin-T and tropomyosin were used at a 1:5000 dilution; and antibody against myosin was used at a 1:1000 dilution. Secondary antibodies were diluted 1:2000 for the detection of actin, myosin, myosin S1, and recombinant vinculin fragments; 1:10 000 for detection of troponin-T and tropomyosin; and 1:5000 for detection of talin.

Gel Electrophoresis and Immunoblot. All proteins used were checked for purity and integrity by SDS−polyacrylamide gel electrophoresis. Protein solutions were mixed 1:1 with 2% sodium dodecyl sulfate (SDS), 20% glycerol, 140 mM β-mercaptoethanol, and 0.05% bromophenol blue. Samples (1−5 μg/lane) were boiled for 2−3 min and separated on gels containing a 4−15% gradient of acrylamide using the Laemmli buffer system (*21*). Duplicate loadings were used for total protein detection with Coomassie brilliant blue and for transblotting. After electrophoresis, proteins were blotted onto polyvinylidenedifluoride (PVDF) membrane in a buffer of 25 mM Tris (pH 8.3), 192 mM glycine, 20% methanol, and 0.1% SDS. Transblotting was performed in a Mini Trans-Blot Electrophoretic Transfer Cell (BioRad Laboratories, Inc., Hercules, CA) at room temperature for 1−2 h at 200 mA. The blotted proteins were incubated with primary and secondary antibodies at the same concentrations used in the ELISA assays (see below) and detected with the ECL Western Blot System (Amersham Corp., Arlington Heights, IL) as previously described (*1*).

ELISA Assays. Nunc MaxiSorp microtiter plates (Nalge Nunc International Corp., Rochester, NY) were coated with purified recombinant N-RAP fragments, HIS-CAT, or bovine serum albumin (BSA). Individual wells were incubated overnight at 4 °C with 100 μL of purified coating proteins at a concentration of 0.1 μM in 6 M urea, 50 mM Tris-HCl (pH 8.0), 5 mM EGTA, and 10 mM dithiothreitol (DTT). Each well was then blocked for 1−3 h at 37 °C with 250 μL of 0.5% BSA in PBS-T (phosphate-buffered saline, pH 7.4, plus 0.2% Tween-20). Wells were incubated overnight at 4 °C with varying concentrations of individual target proteins dissolved in an overlay buffer containing 100 mM KCl, 50 mM Tris-HCl (pH 7.4), 1 mM EGTA, 2 mM $MgCl_2$, 2 mM ATP, 0.3 mM DTT, and 0.2% Tween-20. After incubation, the wells were washed 4 times with PBS-T (250 μL/well, at least 1 min/wash). Primary antibodies (100 μL/well, in PBS-T plus 0.5% BSA) were added and incubated for 1 h at room temperature, followed by another four washes with PBS-T. Incubation with horseradish peroxidase-conjugated secondary antibodies (100 μL/well, in PBS-T plus 0.5% BSA) was at room temperature for 1 h, followed by four washes with PBS-T. Bound horseradish peroxidase-conjugated secondary antibodies were detected by incubating the wells for 30 min with 100 μL of substrate solution (0.1 mg/mL 3,3′,5,5′-tetramethylbenzidine dihydrochloride, 0.01% H_2O_2, and 0.1 M sodium acetate, pH 5.2). The reaction was stopped with the addition of an equal volume of 1 M H_2SO_4. Color development was quantitated by measuring the absorbance at 450 nm using a Dynatech ELISA plate reader (DYNEX Technologies, INC., Chantilly, VA). Each measurement was the result of triplicate or quadruplicate wells.

In some experiments, the concentration of coating proteins was varied and the relative amounts of the histidine-tagged proteins coated onto the plates were determined. The coated and BSA-blocked wells were incubated for 1 h with horseradish peroxidase-linked Ni−NTA conjugates (Qiagen, Inc., Chatsworth, CA) at a dilution of 1:2000 in PBS-T plus 0.5% BSA. This was followed by four washes with PBS-T and the color detection procedure as described above. Finally, the linearity of the assays was evaluated by varying the concentration of coating proteins, and detecting binding of the maximum concentration of target proteins as described above.

Data Analysis. Each data point was the mean of at least three identically treated wells. OD readings from wells in which overlay proteins were omitted are due to nonspecific binding of detection reagents, and were subtracted from each point. (The level of this subtracted background varied depending upon the specific combination of coating protein and detection antibodies. In cases where specific binding of overlay proteins was detected, the subtracted background OD ranged from approximately 10% to 60% of the total OD measured at the maximum concentration of overlay protein

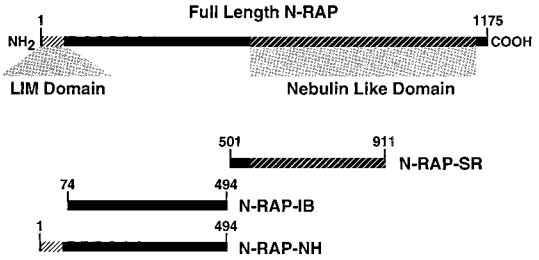

FIGURE 1: Schematic diagram showing the domain organization of N-RAP (top), along with the regions of N-RAP expressed as histidine-tagged fusion proteins. Numbers refer to amino acid residues from the full-length mouse N-RAP sequence (*1*).

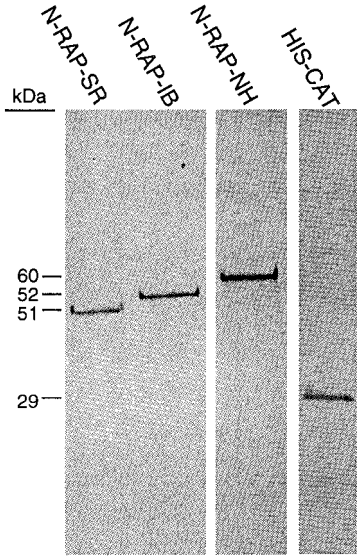

FIGURE 2: Coomassie-stained gel loaded with purified recombinant proteins, as indicated. Each protein migrates as a single band at the size predicted from the DNA sequence.

tested.) OD readings from wells coated with BSA were then subtracted from measurements of wells coated with the target proteins. The resulting values represent specific binding of the overlay protein to the target proteins coating the wells. The values obtained for each overlay protein were normalized to the maximum specific binding obtained for that overlay protein. All points shown are the mean normalized values of at least three independent experiments. The mean data were fit by a simple binding equation: $OD = (OD_{max} \times C/K_d)/(1 + C/K_d)$ where OD is the mean normalized OD, C is the concentration of overlaid test protein, and K_d is the apparent dissociation constant. Data analysis and curve fits were performed on Power Macintosh computers using Kaleidagraph software (Synergy Software, Reading, PA).

RESULTS

Proteins and Antibodies. Figure 1 illustrates the domain organization of N-RAP, as well as the regions of N-RAP that were expressed as histidine-tagged fusion proteins. The fusion proteins are N-RAP-SR, which includes more than 10 complete modules from the nebulin-related super repeat region of N-RAP; N-RAP-IB, which includes most of the region between the nebulin-like region and the LIM domain; and N-RAP-NH, which is an extension of N-RAP-IB to include the N-terminal LIM domain. Figure 2 shows a Coomassie-stained polyacrylamide gel loaded with the purified recombinant N-RAP proteins, as well as with the histidine-tagged chloramphenicol acetyltransferase protein (HIS-CAT). Each of these proteins migrates as a single band at the molecular weight predicted from the DNA sequence of the corresponding recombinant expression plasmid.

We also examined the purity and integrity of each of the proteins tested for N-RAP binding activity, as well as the specificities of the antibodies used to detect these proteins. The resulting gel patterns illustrate that the subunits of the proteins tested were reasonably intact (Figure 3, left-hand panels for each protein). Furthermore, each protein was specifically stained by the appropriate antibody, while other proteins present as markers were not detected (Figure 3, right-hand panels). However, some degradation was observed in the preparations of GST-tagged vinculin fragments. The major breakdown product in these preparations is detected by the anti-GST antibody and migrates at approximately 30 kDa, which is approximately the size of the GST moiety.

Plate Coating. In experiments to assess the relative efficiency with which the various coating proteins bind to the microtiter wells, the concentration of protein present during well-coating was varied. The proteins bound to the wells were then detected using peroxidase-conjugated Ni−NTA, which specifically binds to the histidine tag present in each of the recombinant proteins. These experiments show that the amount of protein bound to the surface is linearly related to the concentration of protein present during the coating step (Figure 4). Furthermore, this relation is similar for all of the coating proteins, indicating that the amount of histidine tag bound to the surface varies less than 20% between proteins. These results show that the molar efficiency of coating is similar for each protein. Therefore, for any particular overlay protein tested, the relative affinity and extent of binding to the various coating proteins can be directly compared.

N-RAP Interaction with Myofibrillar Proteins. A number of myofibrillar proteins were screened for interaction with recombinant N-RAP fragments in solid-phase ELISA assays. Of these, only actin exhibited high-affinity binding to N-RAP fragments. As illustrated in Figure 5, actin binds to all three of the N-RAP fragments tested, with binding appearing to saturate at the same level in each case. However, actin binding to N-RAP-SR is 10-fold stronger than binding to the other N-RAP fragments, with an apparent dissociation constant of 41 nM. The binding curves for actin binding to N-RAP-NH and N-RAP-IB are indistinguishable (Figure 5, open symbols), indicating that actin does not bind to the LIM domain of N-RAP. Since actin binds to all of the recombinant N-RAP fragments tested, we also measured binding to a control protein, HIS-CAT, which contains the same histidine tag that is present in the N-RAP constructs. Binding to HIS-CAT is low and barely distinguishable from the background signal obtained from wells coated with BSA (Figure 5, crosses).

We also screened myosin, tropomyosin, and reconstituted troponin complex for binding to the recombinant N-RAP fragments (Figure 6). As shown in Figure 6A, myosin exhibits no significant binding to N-RAP fragments. Similar negative results were obtained for isolated myosin heads (data not shown). In contrast, tropomyosin and troponin each exhibit significant binding to all of the recombinant N-RAP fragments; moreover, each of these proteins bound equally

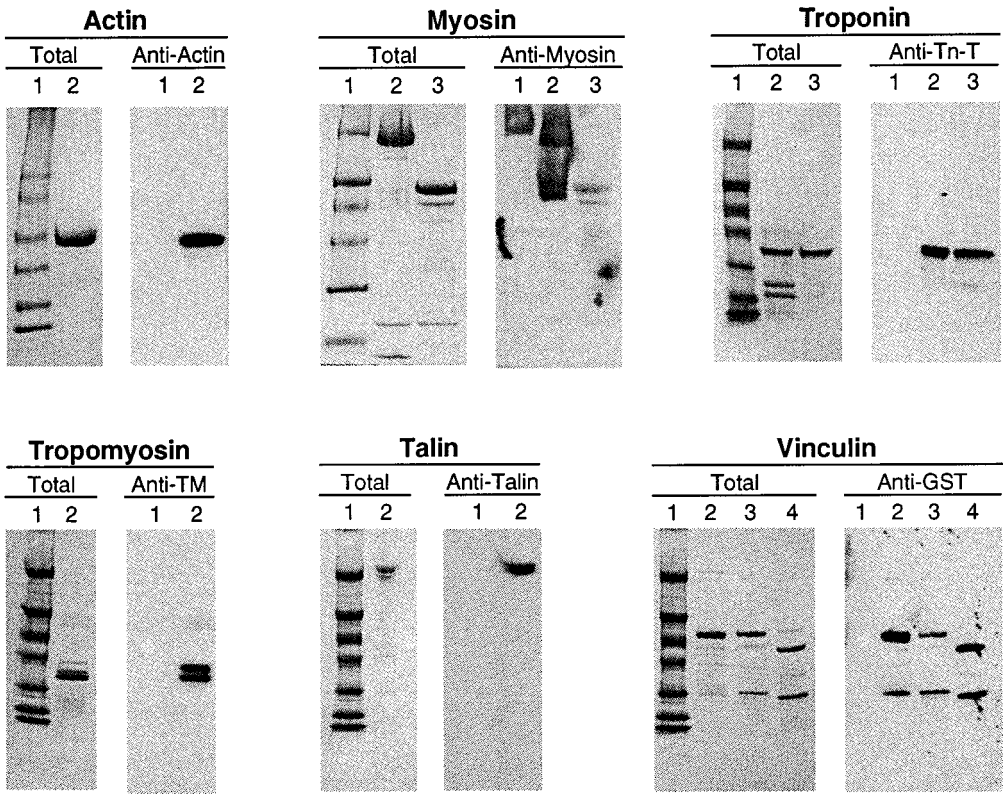

FIGURE 3: Gel electrophoresis and immunoblot of proteins tested for N-RAP binding activity. Each set of panels shows a Coomassie-stained gel (left panels) and corresponding immunoblot (right panels). The first lane in each panel was loaded with a set of molecular weight markers, which serve as negative controls on the blots. Lanes numbered 2 were loaded with the protein indicated above each panel set, except for the vinculin panels. For vinculin, lanes 2, 3, and 4 were loaded with GST/V1−430, GST/V431−850, and GST/V811−1066, respectively. For the myosin and troponin panels, lanes numbered 3 were loaded with myosin subfragment-1 and troponin-T, respectively. Each purified protein was specifically detected using the primary antibody indicated above the blots. Note that myosin heavy chain present in the marker lane was detected by the anti-myosin antibody, while myosin light chains were not detected. Likewise, the anti-troponin-T antibody detected troponin-T, but did not detect the faster migrating troponin-C and troponin-I subunits. The anti-GST antibodies specifically detected the intact vinculin fusion proteins, as well as a prominent breakdown product present in the preparations. Note that the anti-talin antibody detected intact talin as well as the slightly smaller proteolytic fragments that are visible in the Coomassie-stained gel; although these distinct bands are visible in shorter exposures of the illustrated immunoblot, they are not resolved in the longer exposure shown in this figure.

to all of the recombinant N-RAP fragments, with no discernible specificity (Figure 6B,C). We found that binding of tropomyosin and troponin to the HIS-CAT control protein equaled or exceeded binding to the recombinant N-RAP fragments, suggesting that the interactions observed were due to binding to the histidine tag that is present in all of the recombinant coating proteins.

N-RAP Interaction with Junctional Proteins. We screened talin and vinculin, major protein components of the myotendon junction and the intercalated disk, for the ability to bind to N-RAP fragments. Talin exhibited specific binding to N-RAP-NH, the LIM domain containing fragment of N-RAP (Figure 7, open squares). While talin also exhibited a small amount of binding to the other N-RAP fragments, the amount of this binding was highly variable and on average 5-fold less than binding to N-RAP-NH (Figure 7, circles). The interaction of talin with N-RAP-NH is consequently specific and tight, with an apparent dissociation constant of 10 nM.

We tested recombinant fragments of vinculin fused to an N-terminal GST moiety for binding to recombinant N-RAP fragments. Taken together, the three GST fusion proteins cover the entire sequence of chicken vinculin. Initial experiments showed no significant binding of GST itself to N-RAP fragments (data not shown). However, each of the recombinant vinculin proteins exhibited significant and reproducible binding to the recombinant N-RAP fragments (Figure 8A−C). However, GST/V1−430 and GST/V431−850 each bind to HIS-CAT to approximately the same extent as they bind to the recombinant N-RAP proteins (Figure 8A,B), suggesting that the interactions observed for these vinculin fragments are with the histidine tag that is present in each of the coating proteins. The C-terminal-containing vinculin construct, GST/V811−1066, also binds equally well to N-RAP-IB, N-RAP-NH, and HIS-CAT (Figure 8C). However, binding of GST/V811−1066 to N-RAP-SR is significantly greater than binding to the other fragments. Figure 8D shows the binding data for GST/V811−1066 to N-RAP-SR after subtracting the values for binding to HIS-CAT. The data indicate that there is a specific, high-affinity interaction between N-RAP-SR and the C-terminal region of vinculin, with a dissociation constant of 8 nM.

Ionic Strength Dependence of N-RAP Interactions. N-RAP is predicted to be highly basic along its entire length, with calculated isoelectric points for N-RAP-SR, N-RAP-IB, and N-RAP-NH ranging from pH 9.2 to 9.4. Since actin, talin, and vinculin each exhibit differential binding to the various N-RAP regions tested, the observed interactions are more specific than simple binding between oppositely charged proteins. Nevertheless, we sought to assess the importance

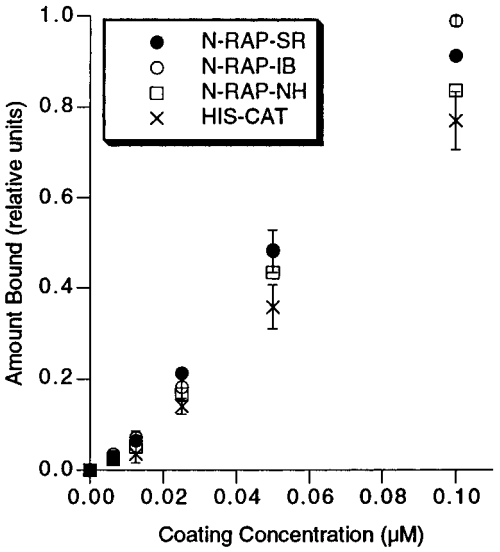

FIGURE 4: Amount of protein coating microtiter wells as a function of the concentration of protein present during coating. Immobilized recombinant proteins were directly detected with horseradish peroxidase linked Ni−NTA, which specifically binds to the histidine tag present in each of the recombinant proteins. The amount of histidine tag bound to the surface increases with the concentration of protein present during the coating step, and is similar for all of the coating proteins. Standard errors are shown for N-RAP-IB and HIS-CAT, and are similar for the other proteins.

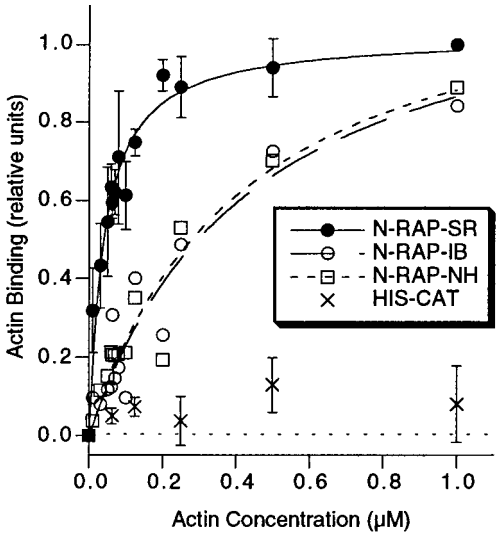

FIGURE 5: Actin binding to the indicated recombinant proteins. The curves are best fits to a simple binding equation, corresponding to an apparent K_d of 41 ± 6 nM, 440 ± 140 nM, and 420 ± 110 nM for binding to N-RAP-SR, N-RAP-IB, and N-RAP-NH, respectively. Standard errors are shown for N-RAP-SR and HIS-CAT, and are similar for the other proteins.

of interactions between charged groups by observing the effect of ionic strength. For these experiments, overlay proteins were present at concentrations sufficient to achieve maximum binding in the standard overlay buffer, and ionic strength was increased by varying the concentration of KCl present during binding.

The results of these experiments are summarized in Figure 9. Actin binding to N-RAP-SR was eliminated as the KCl concentration increased from 100 to 500 mM, while actin binding to N-RAP-NH was less sensitive, decreasing 40% over this range. Talin binding to N-RAP-NH decreased 50% as the KCl concentration increased, while binding of the

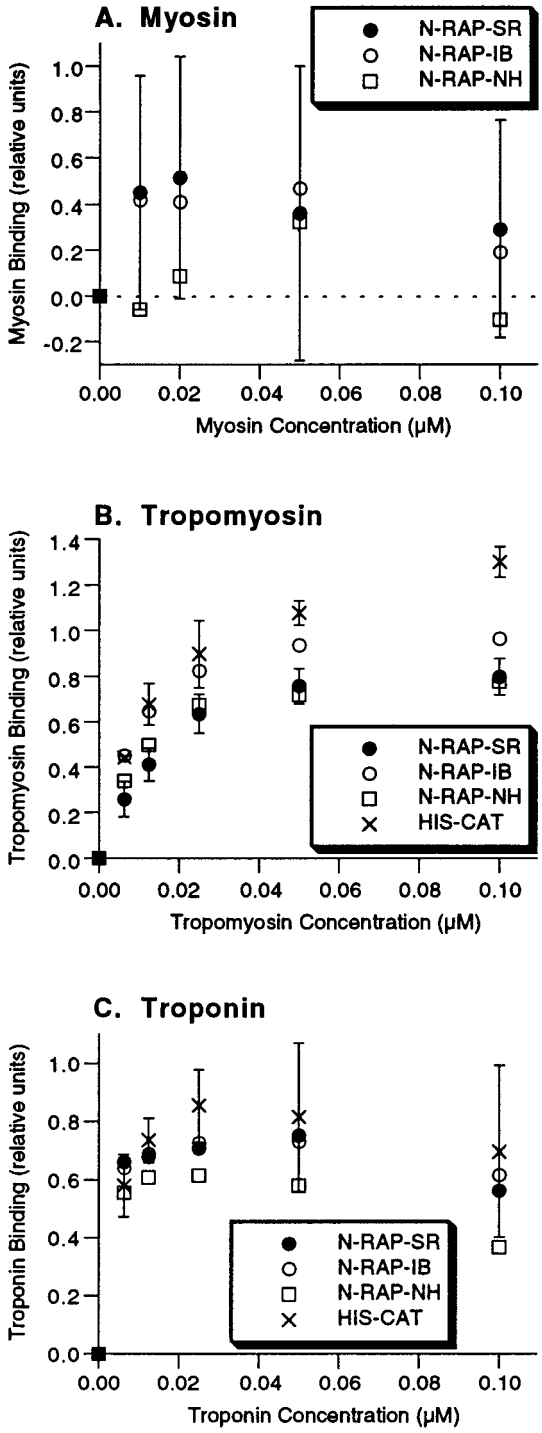

FIGURE 6: Binding of myosin (A), tropomyosin (B), and troponin (C) to the indicated recombinant proteins. No significant binding of myosin was observed. Tropomyosin and troponin binding to the recombinant N-RAP proteins was significantly above background, but did not exceed binding to the HIS-CAT control protein. Standard errors are shown for N-RAP-SR and HIS-CAT, and are similar for the other proteins. Note that the normalization procedure artificially expands the scale when no significant binding is observed, as for myosin (A).

C-terminal region of vinculin, GST/V811−1066, increased 2-fold over this range.

Assay Linearity. We assessed the linearity of the assays for each combination of primary and secondary antibodies used to detect bound test protein. This was accomplished by varying the concentration of target protein present during well coating, which is linearly related to the amount of

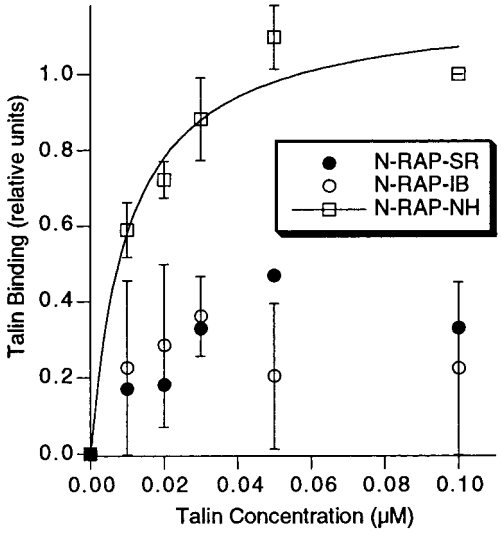

FIGURE 7: Binding of talin to the indicated recombinant proteins. Significant binding was observed to N-RAP-NH, with a best fit to a simple binding equation yielding an apparent K_d of 10 ± 3 nM. Binding to N-RAP-IB and N-RAP-SR is just barely above background. Standard errors are shown for N-RAP-NH and N-RAP-IB, and are similar for N-RAP-SR.

protein coated onto the wells (see Figure 4). A maximum concentration of test protein was then used during the overlay step. Figure 10 shows that for actin, talin, and vinculin detection, there is a reasonably linear relation between coating concentration and detection of bound test protein at apparently saturating concentrations. The results show that these assays are reasonably linear over the range of protein concentrations used, and that the saturation of binding that was observed for these proteins was not due to an exhaustion of any of the reagents used for detecting bound protein.

DISCUSSION

Our results demonstrate high-affinity binding of defined regions of N-RAP to actin, talin, and vinculin. Extremely tight binding of both actin and vinculin to the super repeat region of N-RAP was observed. In addition, we detected a high-affinity interaction between the N-RAP LIM domain and talin.

Properties of the Assay. We used a nonequilibrium method for measuring the relative amounts of overlay proteins bound to target proteins immobilized on a solid surface. Because the efficiency with which the various recombinant proteins coated the microtiter wells was similar, quantitative comparisons could be made between the binding of a single overlay protein to the various coating proteins. The assays were also shown to be fairly linear.

Although this assay allowed us to efficiently screen a large number of proteins for binding to N-RAP domains, several limitations must be kept in mind when interpreting the data. First, because the recombinant N-RAP fragments have limited solubility, proteins were coated onto the wells in the presence of urea; during subsequent washing, blocking, and binding steps, the immobilized proteins must refold to an extent that is sufficient for specific binding of the test proteins to be observed. Second, there was ample opportunity for bound overlay proteins to be released during subsequent wash steps. Therefore, the method can only detect interactions with relatively slow unbinding kinetics. The assays are therefore sufficient to explore high-affinity interactions with long lifetimes, but will not detect transient complexes that rapidly dissociate. Finally, any binding observed may actually be tighter than indicated by the apparent dissociation constants, since neither a decrease in free ligand concentration due to binding nor dissociation during subsequent washing was considered in fitting the data.

Actin Binding. The extent of actin binding was similar for each of the recombinant N-RAP fragments used in this study. However, actin binding to N-RAP-SR was much stronger than to the other N-RAP constructs, exhibiting an apparent dissociation constant of 41 nM. This is well below the critical concentration for actin polymerization, suggesting that the N-RAP repeats bind monomeric actin. [Using a sedimentation assay for actin polymerization, we measured a critical concentration of 0.3 μM in the same buffer used for the ELISA binding assays (data not shown).] These results are consistent with our previous finding that actin at submicromolar concentrations binds to N-RAP-SR and nebulin repeats in a gel overlay assay, while only a trace amount of actin binding to N-RAP-IB was observed (*1*). The high-affinity interaction of actin with N-RAP-SR is also consistent with previous studies using synthetic nebulin peptides and recombinant nebulin repeats. These studies showed that individual nebulin modules bind to actin rather weakly, with dissociation constants ranging from 40 to 500 μM or higher (*22*, *23*), while recombinant nebulin fragments containing several modules generally bind to actin with dissociation constants in the submicromolar range (*4*, *24*−*26*). Interestingly, nebulin fragments containing two or six modules are capable of stabilizing actin nuclei and of rendering actin polymerizable under normally nonpolymerizing conditions (*27*, *28*). These results suggest the possibility that the actin bound to N-RAP-SR was stabilized in a filamentous form, even at concentrations below that needed for the polymerization of pure actin.

Although it has limited sequence similarity to nebulin, N-RAP-IB is, like nebulin and the nebulin-related region of N-RAP, highly basic (*1*), and exhibits an actin binding affintity that is 10-fold weaker than actin binding to N-RAP-SR. Actin binding to N-RAP-NH was indistinguishable from its binding to N-RAP-IB, indicating that actin does not bind to the N-RAP LIM domain. The range of concentrations over which actin binding to N-RAP-IB increased is consistent with binding of both monomeric and filamentous actin.

Talin Binding. Our data demonstrate a high-affinity interaction between human talin and the N-RAP LIM domain. Previous studies have demonstrated a direct interaction between talin and actin (*29*−*31*), as well as between talin and integrin (*32*−*34*). Talin alone can therefore in principle provide a direct bridge between actin filaments and an integral membrane protein.

Vinculin Binding. Three recombinant vinculin fragments, which together represent the entire vinculin molecule, were tested for binding to N-RAP domains. Of these, the C-terminal construct containing residues 811−1066 of chicken vinculin exhibited specific, saturable binding to the super repeat region of N-RAP. This region of vinculin contains the entire 30 kilodalton tail domain, as well as the extreme C-terminus of the 95 kilodalton head domain. In addition to the high-affinity interaction with N-RAP super repeats reported here, the vinculin tail domain binds actin (*15*, *35*,

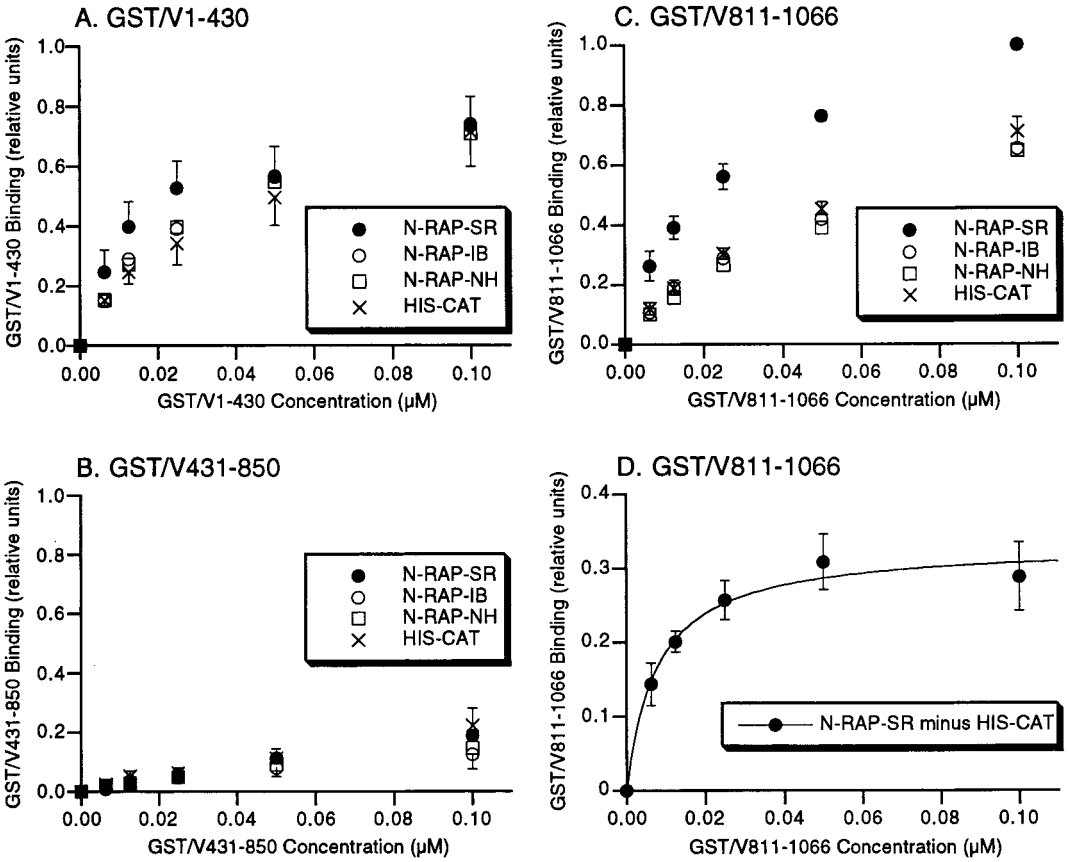

FIGURE 8: Binding of GST/vinculin fusion proteins to the indicated recombinant proteins. GST/V1−430 (A) and GST/V431−850 (B) binding to the recombinant N-RAP proteins was significantly above background, but did not consistently exceed binding to the HIS-CAT control protein. GST/V811−1066 bound similarly to N-RAP-IB, N-RAP-NH, and the HIS-CAT control protein, but increased binding to N-RAP-SR was observed (C). Panel D shows the specific binding of GST/V811−1066 to N-RAP-SR after subtracting the binding to HIS-CAT. These data are well fit by a simple binding equation, yielding an apparent K_d of 7.7 ± 1.5 nM. Standard errors are shown for N-RAP-SR and HIS-CAT (A and C) or for N-RAP-IB and HIS-CAT (B), and are similar for the other proteins in each panel.

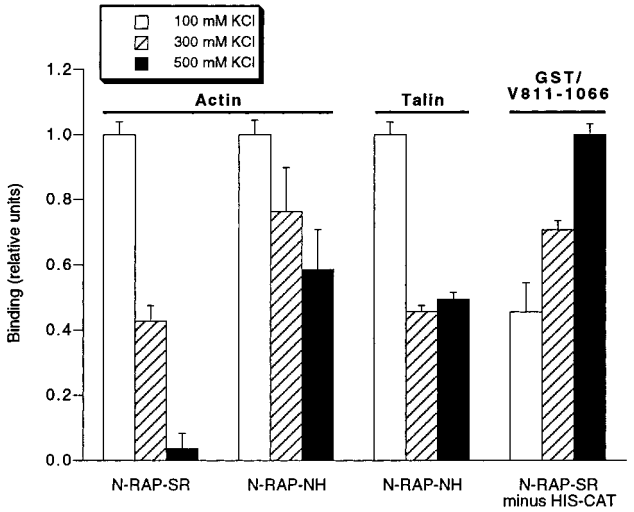

FIGURE 9: Ionic strength dependence of the binding of the indicated overlay proteins to the indicated N-RAP fragments. Actin (1 μM), talin (0.075 μM), and GST/V811−1066 (0.1 μM) incubations were in overlay buffer containing 100, 300, and 500 mM KCl.

36), paxillin (*37*, *38*), and acidic phospholipids (*39*), while the head region of vinculin binds talin (*40*−*42*). Interestingly, an intramolecular association between the head and tail domains of vinculin inhibits their interaction with talin and actin, respectively (*15*, *41*). Regulation of the intramolecular vinculin head−tail interaction has been proposed as a mechanism to control recruitment and assembly of vinculin in focal adhesions. This proposal is supported by the finding that the interaction between the vinculin head and tail domains is inhibited by acidic phospholipids (*43*) and the second messenger phosphatidylinositol 4,5-bisphosphate (*42*). Disruption of this intramolecular interaction in turn unmasks the binding sites for talin (*42*) and actin (*42*, *43*), as well as a site phosphorylated by protein kinase C (*43*). It remains to be determined if the interaction between vinculin and N-RAP is similarly regulated, or if N-RAP binding affects the interaction between vinculin and its other ligands.

Myotendon Junctions, Intercalated Disks, and Focal Adhesions. Myotendon junctions, intercalated disks, and focal adehesions are each specialized attachment sites for tension-bearing structures. The intracellular face of myotendon junctions and intercalated disks are the sites of myofibril attachment to the cell membrane in skeletal and cardiac muscle cells, respectively (*11*, *12*). These sites contain many proteins that are also present at focal contacts formed between cultured cells and the underlying substrate (*44*, *45*), including talin (*13*) and vinculin (*14*). The ends of striated muscles can therefore be thought of as extremely stable focal adhesions specifically adapted to transmit the large forces produced by the myofibrils.

One such adaptation is in the particular form of integrin found at the junctional sites. Muscle cells contain a specific splice varient of the β1-integrin subunit, β1D, that is concentrated at myotendon junctions in skeletal muscle and

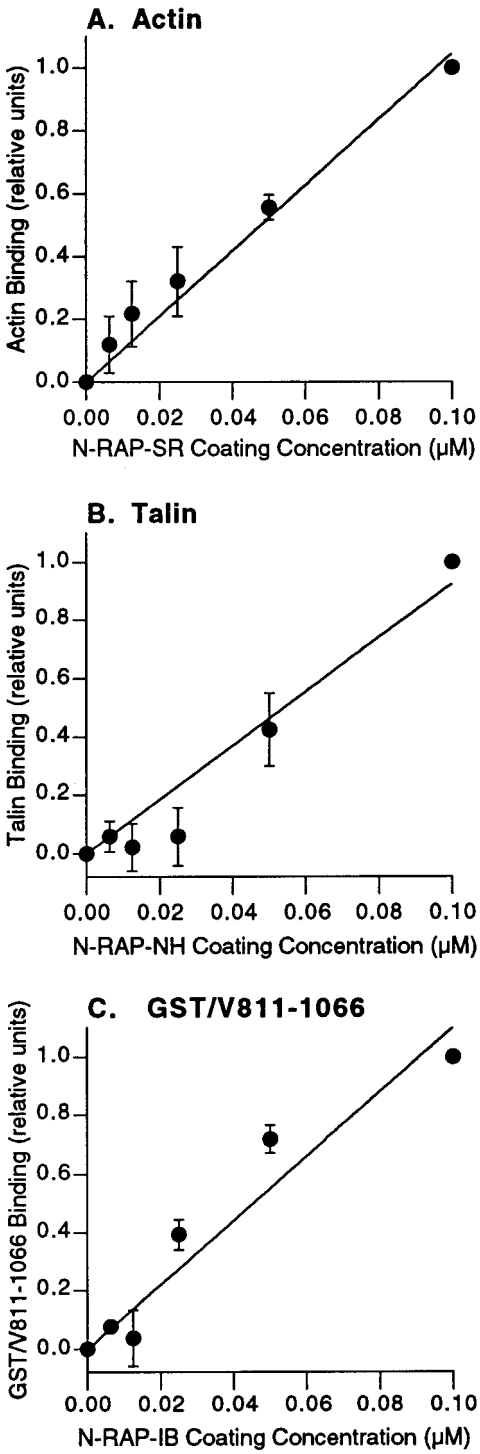

FIGURE 10: Maximum protein binding versus coating concentration. Microtiter wells were coated with varying concentrations of N-RAP-SR (A), N-RAP-NH (B), or N-RAP-IB (C). They were then overlayed with 1 μM actin (A), 0.1 μM talin (B), or 0.1 μM GST/V811−1066 (C). In each case, the relative binding detected is linearly related to the amount of target protein coated onto the wells, as expected for a linear assay.

at intercalated disks in cardiac muscle (*46*). Binding to talin is severalfold stronger for the cytoplasmic domain of β1D integrin than for the more ubiquitous β1A isoform (*47*). Furthermore, nonmuscle cells transformed with β1D integrin exhibit increased contractility, without increased activation of the contractile apparatus as measured by myosin light chain phosphorylation (*47*). No increase in contractilty was observed in cells transformed with β1A integrin (*47*).

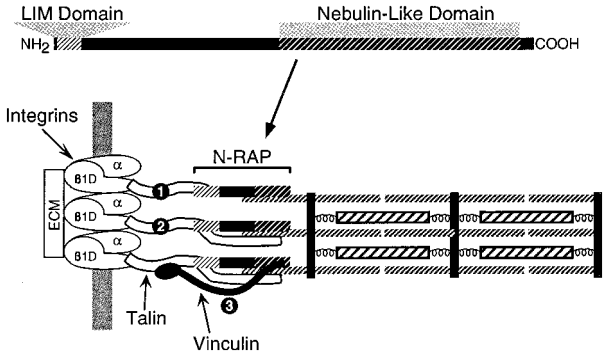

FIGURE 11: Some possible schemes for linking the terminal actin filaments of myofibrils to the cell membrane. The domain organization of N-RAP is shown at the top, with distinct hatch patterns marking the positions of the nebulin-related region and the LIM domain. These domains are shown binding to the terminal actin filaments and to talin, respectively; talin in turn binds to the β1D integrin subunit, completing the linkage between the myofibril and the plasma membrane (numeral 1). Interactions between talin and actin filaments (numeral 2) and between vinculin and talin, actin, and N-RAP (numeral 3) are sequentially added. The integrins transmit tension produced by cytoplasmic structures to the extracellular matrix (ECM).

Alternative splicing therefore produces a muscle-specific integrin isoform that enhances cellular contractility by producing more stable attachments between actin filaments and the plasma membrane.

N-RAP may represent a second adaptation of junctional regions in muscle cells for transmission of large forces to the extracellular matrix. Unlike talin and vinculin, N-RAP is specifically expressed in skeletal and cardiac muscles (*1*). The N-RAP super repeats bind actin very tightly (this report), and, by analogy with nebulin (*4*, *23*), probably include several distinct binding sites for actin filaments. N-RAP binding to actin filaments should therefore be highly cooperative and stable, and may be essential for transmitting the large tensions produced during myofibril contraction.

Figure 11 illustrates some established molecular interactions that could serve to link the terminal actin filaments of myofibrils to the cell membrane. In these schemes, the N-RAP super repeats bind tightly to the terminal actin filaments, while the N-RAP LIM domain binds strongly to talin; talin binding to the β1D integrin subunit completes the mechanical linkage between the myofibrils and the membrane (Figure 11, Scheme 1). More complicated assemblies are also consistent with the binding data. For example, talin may bind simultaneously to actin filaments and the N-RAP LIM domain (Figure 11, Scheme 2), or vinculin could form a parallel linkage between the actin−N-RAP complex and talin (Figure 11, Scheme 3). Future studies will determine if any of the schemes presented in Figure 11 are correct, or if more complex assemblages must be considered.

ACKNOWLEDGMENT

We are indebted to our colleagues for generous gifts of purified proteins. We thank Dr. Susan W. Craig (Johns Hopkins University) for providing GST-tagged recombinant chicken vinculin fragments, Dr. Keith Burridge (University of North Carolina) for purified human talin, Dr. James Sellers (NHLBI, National Institutes of Health) for actin purified from rabbit skeletal muscle, Dr. Mingda She (NIAMS, National

Institutes of Health) for purified rabbit tropomyosin, troponin-T, and reconstituted troponin complex, and Dr. Ling Xie (NIAMS, National Institutes of Health) for rabbit myosin and isolated myosin heads.

REFERENCES

1. Luo, G., Zhang, J. Q., Nguyen, T. P., Herrera, A. H., Paterson, B., and Horowits, R. (1997) *Cell Motil. Cytoskeleton 38*, 75−90.
2. Labeit, S., Gibson, T., Lakey, A., Leonard, K., Zeviani, M., Knight, P., Wardale, J., and Trinick, J. (1991) *FEBS Lett. 282*, 313−316.
3. Labeit, S., and Kolmerer, B. (1995) *J. Mol. Biol. 248*, 308−315.
4. Wang, K., Knipfer, M., Huang, Q.-Q., van Heerden, A., Hsu, L. C.-L., Gutierrez, G., Quian, X.-L., and Stedman, H. (1996) *J. Biol. Chem. 271*, 4304−4314.
5. Zhang, J. Q., Luo, G., Herrera, A. H., Paterson, B., and Horowits, R. (1996) *Eur. J. Biochem. 239*, 835−841.
6. Wright, J., Huang, Q. Q., and Wang, K. (1993) *J. Muscle Res. Cell Motil. 14*, 476−483.
7. Kruger, M., Wright, J., and Wang, K. (1991) *J. Cell Biol. 115*, 97−107.
8. Sanchez, G. I., and Rabbitts, T. H. (1994) *Trends Genet. 10*, 315−320.
9. Dawid, I. B., Toyama, R., and Taira, M. (1995) *C. R. Acad. Sci. III 318*, 295−306.
10. Forbes, M. S., and Sperelakis, N. (1985) *Tissue Cell 17*, 605−648.
11. Severs, N. J. (1990) *Int. J. Cardiol. 26*, 137−173.
12. Tidball, J. G. (1991) *J. Biomech. 24 Suppl. 1*, 43−52.
13. Tidball, J. G., O'Halloran, T., and Burridge, K. (1986) *J. Cell Biol. 103*, 1465−1472.
14. Shear, C. R., and Bloch, R. J. (1985) *J. Cell Biol. 101*, 240−256.
15. Johnson, R. P., and Craig, S. W. (1995) *Nature 373*, 261−264.
16. Adey, N. B., and Kay, B. K. (1997) *Biochem. J. 324*, 523−528.
17. Turner, C. E., and Burridge, K. (1989) *Eur. J. Cell Biol. 49*, 202−206.
18. Eisenberg, E., and Kielley, W. W. (1974) *J. Biol. Chem. 249*, 4742−4748.
19. Potter, J. D. (1982) *Methods Enzymol. 85*, 241−263.
20. Xie, L., and Schoenberg, M. (1998) *Biochemistry 37*, 8048−8053.
21. Laemmli, U. K. (1970) *Nature 227*, 680−685.
22. Pfuhl, M., Winder, S. J., and Pastore, A. (1994) *EMBO J. 13*, 1782−1789.
23. Pfuhl, M., Winder, S. J., Castiglione Morelli, M. A., Labeit, S., and Pastore, A. (1996) *J. Mol. Biol. 257*, 367−384.
24. Jin, J. P., and Wang, K. (1991) *J. Biol. Chem. 266*, 21215−21223.
25. Root, D. D., and Wang, K. (1994) *Biochemistry 33*, 12581−12591.
26. Zhang, J. Q., Weisberg, A., and Horowits, R. (1998) *Biophys. J. 74*, 349−359.
27. Chen, M. J., Shih, C. L., and Wang, K. (1993) *J. Biol. Chem. 268*, 20327−20334.
28. Gonsior, S. M., Gautel, M., and Hinssen, H. (1998) *J. Muscle Res. Cell Motil. 19*, 225−235.
29. Hemmings, L., Rees, D. J., Ohanian, V., Bolton, S. J., Gilmore, A. P., Patel, B., Priddle, H., Trevithick, J. E., Hynes, R. O., and Critchley, D. R. (1996) *J. Cell Sci. 109*, 2715−2726.
30. Zhang, J., Robson, R. M., Schmidt, J. M., and Stromer, M. H. (1996) *Biochem. Biophys. Res. Commun. 218*, 530−537.
31. Muguruma, M., Matsumura, S., and Fukazawa, T. (1990) *Biochem. Biophys. Res. Commun. 171*, 1217−1223.
32. Horwitz, A., Duggan, K., Buck, C., Beckerle, M. C., and Burridge, K. (1986) *Nature 320*, 531−533.
33. Buck, C. A., and Horwitz, A. F. (1987) *J. Cell Sci. Suppl. 8*, 231−250.
34. Pfaff, M., Liu, S., Erle, D. J., and Ginsberg, M. H. (1998) *J. Biol. Chem. 273*, 6104−6109.
35. Huttelmaier, S., Bubeck, P., Rudiger, M., and Jockusch, B. M. (1997) *Eur. J. Biochem. 247*, 1136−1142.
36. Menkel, A. R., Kroemker, M., Bubeck, P., Ronsiek, M., Nikolai, G., and Jockusch, B. M. (1994) *J. Cell Biol. 126*, 1231−1240.
37. Turner, C. E., Glenney, J. R., Jr., and Burridge, K. (1990) *J. Cell Biol. 111*, 1059−1068.
38. Wood, C. K., Turner, C. E., Jackson, P., and Critchley, D. R. (1994) *J. Cell Sci. 107*, 709−717.
39. Johnson, R. P., and Craig, S. W. (1995) *Biochem. Biophys. Res. Commun. 210*, 159−164.
40. Price, G. J., Jones, P., Davison, M. D., Patel, B., Bendori, R., Geiger, B., and Critchley, D. R. (1989) *Biochem. J. 259*, 453−461.
41. Johnson, R. P., and Craig, S. W. (1994) *J. Biol. Chem. 269*, 12611−12619.
42. Gilmore, A. P., and Burridge, K. (1996) *Nature 381*, 531−535.
43. Weekes, J., Barry, S. T., and Critchley, D. R. (1996) *Biochem. J. 314*, 827−832.
44. Burridge, K., and Chrzanowska-Wodnicka, M. (1996) *Annu. Rev. Cell Dev. Biol. 12*, 463−518.
45. Craig, S. W., and Johnson, R. P. (1996) *Curr. Opin. Cell Biol. 8*, 74−85.
46. Belkin, A. M., Zhidkova, N. I., Balzac, F., Altruda, F., Tomatis, D., Maier, A., Tarone, G., Koteliansky, V. E., and Burridge, K. (1996) *J. Cell Biol. 132*, 211−226.
47. Belkin, A. M., Retta, S. F., Pletjushkina, O. Y., Balzac, F., Silengo, L., Fassler, R., Koteliansky, V. E., Burridge, K., and Tarone, G. (1997) *J. Cell Biol. 139*, 1583−1595.

BI982395T